Boundary-Layer Meteorol (2007) 123:1–28
DOI 10.1007/s10546-007-9161-1

ORIGINAL PAPER

# The Energy Balance Experiment EBEX-2000. Part I: overview and energy balance

**Steven P. Oncley · Thomas Foken · Roland Vogt · Wim Kohsiek · H. A. R. DeBruin · Christian Bernhofer · Andreas Christen · Eva van Gorsel · David Grantz · Christian Feigenwinter · Irene Lehner · Claudia Liebethal · Heping Liu · Matthias Mauder · Andrea Pitacco · Luis Ribeiro · Tamas Weidinger**

Received: 13 December 2005 / Accepted: 22 January 2007 / Published online: 14 March 2007


**Abstract** An overview of the Energy Balance Experiment (EBEX-2000) is given. This experiment studied the ability of state-of-the-art measurements to close the surface energy balance over a surface (a vegetative canopy with large evapotranspiration) where closure has been difficult to obtain. A flood-irrigated cotton field over uniform terrain was used, though aerial imagery and direct flux measurements showed that the surface still was inhomogeneous. All major terms of the surface energy balance were measured at nine sites to characterize the spatial variability across the field. Included in these observations was an estimate of heat storage in the plant canopy. The resultant imbalance still was 10%, which exceeds the estimated measurement error. We speculate that horizontal advection in the layer between the canopy top and our flux measurement height may cause this imbalance, though our estimates of

The National Center for Atmospheric Research is supported by the National Science Foundation.

S. P. Oncley (✉)
National Center for Atmospheric Research/ATD,
P.O. Box 3000, Boulder, CO 80307-3000, USA
e-mail: oncley@ucar.edu

T. Foken
University of Bayreuth,
Bayreuth, Germany

R. Vogt · A. Christen · C. Feigenwinter · I. Lehner
University of Basel,
Basel, Switzerland

W. Kohsiek
Royal Netherlands Meteorological Institute (KNMI),
De Bilt, The Netherlands

H. A. R. DeBruin
Meteorology and Air Quality Group, Wageningen University and Research Center,
Wageningen, The Netherlands

this term using our measurements resulted in values less than what would be required to balance the budget.

**Keywords** Flux divergence · Latent heat flux · Spatial sampling · Sensible heat flux · Soil heating · Surface energy budget

## 1 Introduction

Energy must be conserved at the earth's surface, a fundamental fact that is used in all weather and climate models. The major components of the surface energy budget are net radiation $R_{net}$ (in both the visible and infrared part of the spectrum), sensible heat flux $H$ (exchange of heat between the surface and the atmosphere by conduction and convection), latent heat flux $LE$ (evaporation of water from the surface, where L is the latent heat of vaporization), and heating $G$ of materials on the surface (soil, plants, water, etc.), with a small fraction converted to chemical energy when plants are present. Thus,

$$R_{net} = H + LE + G. \tag{1}$$

C. Bernhofer
Dresden University of Technology,
Dresden, Germany

E. van Gorsel
CSIRO,
Canberra, Australia

D. Grantz
University of California, Kearney Research Center,
Parlier, CA, USA

C. Liebethal
e-fellows.net
Munich, Germany

H. Liu
Jackson State University,
Jackson, MS, USA

M. Mauder
Agriculture and Agri-Food
Ottawa, Ont., Canada

A. Pitacco
University of Padova,
Padova, Italy

L. Ribeiro
Bragança Polytechnic Institute,
Bragança, Portugal

T. Weidinger
Eötvös Loránd University,
Budapest, Hungary

**Table 1** Recent energy balance observations

| Experiment | Reference | Residual (%) | Duration (days) | Surface |
|---|---|---|---|---|
| FIFE-89 | Verma et al. (1992) | 0–10 | 40 | grass |
| Vancouver Island-90 | Lee and Black (1993) | 17 | 9 | 16 m deciduous forest |
| TARTEX-90 | Foken et al. (1993) | 33 | 24 | barley/bare soil |
| KUREX-91 | Panin et al. (1998) | 38 | 27 | agricultural |
| LINEX-96/2 | Foken et al. (1997) | 21 | 3 | medium grass |
| LINEX-97/1 | Foken (1998) | 32 | 9 | short grass |
| LITFASS-98 | Beyrich et al. (2002) | 14 | 21 | bare soil |

FIFE is the First International Satellite Land Surface Climatology Project (ISLSCP) Field Experiment, TARTEX is the Tartu Experiment, LINEX is the Lindenberg Experiment, and LITFASS is the Lindenberg Inhomogeneous Terrain – Fluxes between Atmosphere and Surface: a long-term study

Several early measurements of the energy balance terms failed to achieve closure (Elagina et al. 1973, 1978; Tsvang et al. 1987). The problem was more evident during the land surface experiments at the end of the 1980s such as the First International Satellite Land Surface Climatology Project (ISLSCP) Field Experiment (FIFE) (Kanemasu et al. 1992). While the cause was first thought to be in the eddy-covariance measurements, later studies discussed problems with the radiation measurements (Koitzsch et al. 1988) and the storage in the canopy and the upper soil layer (Foken 1990; Bolle et al. 1993; Braud et al. 1993). The lack of closure of the energy balance in the land surface experiments given in Table 1 was interpreted by Foken (1998) as an effect of the fractional coverage of vegetation and the influence of the soil heat storage. The imbalance was attributed by Panin et al. (1998) to the influence of heterogeneities in the surrounding area and by Twine et al. (2000) to unknown problems with the sensible and/or latent heat flux measurements. Finnigan et al. (2003) focused on the problem of inadequate temporal averaging (which would lose low-frequency contributions) for the turbulent fluxes, perhaps related to non-homogeneous surfaces. It also is conceivable that a physical process exists that has not been included in Eq. (1); however we only find one (Sect. 6.3 below) and show that it is negligible.

The lack of energy balance closure has been found over all types of surfaces from bare soil to forests and the vast majority have found higher energy input by radiation fluxes than loss by turbulent fluxes and ground heat flux. Several overview papers are now available (Laubach and Teichmann 1996; Foken 1998; Aubinet et al. 2000; Wilson et al. 2002; Culf et al. 2004) that make the problem well-known. Energy balance closure has been used to characterize the quality of eddy-covariance based fluxes, although other factors such as the choice of coordinate system, the footprints of each of the budget terms, and mesoscale transport can influence the closure (Foken et al. 2004).

The error that is found is much larger than is usually expected for the measurements of any of the individual terms. It is important to determine the reasons for this deficit. Otherwise, it is impossible to use experimental data for, say, the evaluation of subgrid parameterizations of the soil-vegetation-atmosphere transfer schemes in climate numerical models, because it is not known which components of the energy balance may be in error.

The primary objective of the Energy Balance EXperiment (EBEX) was to determine why measurements often cannot achieve closure. EBEX was the direct result of a European Geophysical Society workshop (Foken and Oncley 1995), which listed

both instrumentation and fundamental problems in closing the energy budget. EBEX addressed these problems by:

1. Studying a surface for which energy balance closure has been difficult to obtain, but still relatively easy to instrument—a closed canopy with high evapotranspiration.
2. Measuring all terms of the energy budget directly at comparable scales. In particular, deploying enough sensors to create an average of each term over an area large enough to encompass several flux "footprints".
3. Performing side-by-side intercomparisons of instruments from different manufacturers.
4. Comparing processing methods of different research groups, including filtering and flow distortion corrections in the eddy-covariance measurements, using a reference dataset.

In addition, temperature and wind profiles were measured at three locations to provide information on site homogeneity—in particular the presence or lack of internal boundary layers over the site. It was not expected that point 2 above would be the primary source of the systematic imbalance observed in the past, since sampling could cause $H + LE + G$ to be either larger or smaller than $R_{net}$.

## 2 Site description

We selected a flood-irrigated cotton field in the San Joaquin Valley of California since the typically cloud-free skies resulted in quite high evapotranspiration, with maximum values over 600 W m$^{-2}$. The site was a field 1,600 m × 800 m approximately 20 km south-south-west of the town of Lemoore. The local overall topography was quite flat with a slope of 0.1 degree. The canopy grew during the project and also varied spatially, but was generally 1 m high; the canopy closed at all but sites 9 and 10 during the measurement period.

Winds were quite steady from the north-north-west at upper levels, as shown in Fig. 1, due to channelling of the synoptic flow by mountains surrounding the Valley. Figure 2 shows that these north-north-west winds are perfectly aligned with the topography. The near-surface winds also came from the north-east during the day and from the west at night, probably due to drainage/upslope flows through Cottonwood Pass, about 30 km to the south-west. The influence of topography on the air flow in this area is described in Tanrikulu et al. (2000).

Most flux measurements were made at 4.7 m above the ground (about 4 m above the estimated displacement height) and thus had a fetch (producing 90% of the flux for slightly unstable conditions) of about 400 m (Horst and Weil 1994). The layout of the ten tower sites (Fig. 3) with tower spacing of 200 m was chosen to have this footprint totally within the cotton field and to have overlapping footprints from adjacent towers to identify any sections of the field with significantly different fluxes. The relative orientation of these towers was set to the expected mean wind direction (from the north-north-west) so that these footprints would overlap. Although internal boundary layers were seen, temperature (and to a lesser extent, wind speed) profiles measured at sites 7, 8, and 9 indicated that the measuring level for fluxes was above this layer at most of the stations (except stations 3, 6, 9 for easterly winds).

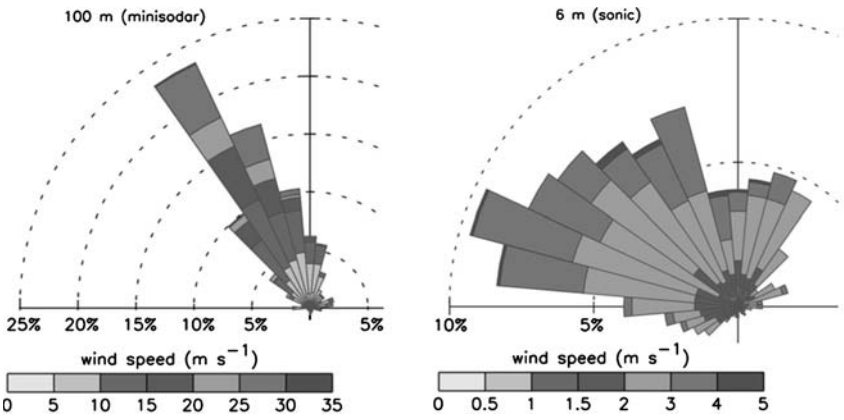


**Fig. 1** Wind directions and speeds measured by a sodar at 100 m and by a sonic anemometer at 6 m

All sites had measurements of momentum, sensible, and latent heat fluxes at one or more heights, soil temperature and moisture, soil heat flux, and net and upwelling visible and infrared radiation. Sites 7, 8, and 9 were enhanced sites that also had wind, temperature, and humidity profile measurements at six or more levels and downwelling visible and infrared radiation. At site 7, sonic anemometers were installed at four heights to investigate vertical flux divergence and at site 9 small-scale horizontal flux divergence was investigated with three additional towers, each with flux measurements at two heights. Canopy heating was measured near sites 9 and 10. For a brief period, soil and canopy heating was measured at four locations along a row just north of site 7 and another four locations along a row north of site 1. Although most of the data from these sensors were acquired by the National Center for Atmospheric Research (NCAR) Integrated Surface Flux Facility (ISFF), the other research groups (at sites 7, 9, and 10) also collected their own data so that data processing methods may be compared. A summary of all these sensors and heights is given in Tables 2–5.

To obtain information about the flow in the valley, we utilized several remote sensors. We deployed a sodar (Scintec FAS64) at the EBEX site that reported backscatter intensity at 1-m resolution and winds at 30-m resolution from heights up to 480 m. We also obtained low-level radial velocities from the National Weather Service 88D radar at Hanford, California while it was operating in clear-air surveillance mode. Finally, our measurement period coincided with the Central California Ozone Study (CCOS) and California Regional Particulate Air Quality Study (CRPAQS) (Wilczak et al. 2004; Soong et al. 2004; Herckes et al. 2002). Among other instrumentation, a network of 915 MHz wind profilers collected data at seven locations within 100 km of our site, with the closest 22 km to the north-east.

The field was flood irrigated over a period of several days (working north to south) twice during the observation period as indicated in Fig. 4. With this schedule, about half of the time the soil moisture was not uniform across the field, though the fluxes were not dramatically different (see below).

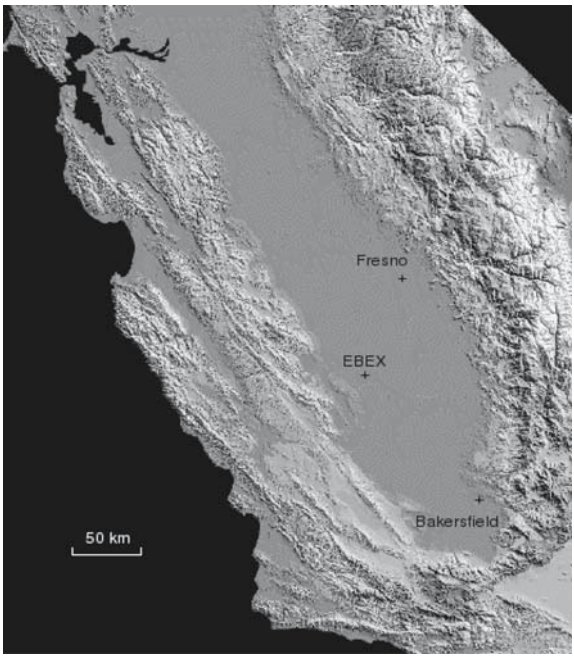


**Fig. 2** Topographic map of the San Joaquin Valley in California. The location of the EBEX site is indicated. Note the general north-north-west to south-south-east alignment of the valley and some small passes to the South of the EBEX site. Base map from the United States Geological Survey (USGS) wwwflag.wr.usgs.gov/USGS-Flag/Data/maps/California.gif

## 3 Operations

EBEX had two operational periods. From 18 to 29 July, representative turbulence sensors were deployed side-by-side for a flux instrument intercomparison (see Mauder et al. 2007, for more details). For the remainder of the study, the sensors were deployed throughout the field to document any horizontal variability. On 14 August, the sensors at site 3 were moved to the bare dirt field just to the north of the cotton field in order to document the characteristics of the upwind flow.

One operational problem was the aerial application of pesticides during the study. Since these were somewhat toxic, personnel were unable to enter the field to service the sensors for 1–3 days after application. However, the pesticides left a residue on the upward-looking radiometers that, in addition to dust deposition, attenuated the incoming radiation. Thus, there were periods of several days for which data had to be discarded.

## 4 Major terms

We now proceed to the investigation of each of the terms in Eq. (1). Since the instrumentation, data issues, and analysis methods are significantly different for each term, we discuss them separately.

### 4.1 Net radiation

Although net radiometers were deployed during EBEX at every site, we expect greater accuracy (Kohsiek et al. 2007) by determining $R_{net}$ from the four components

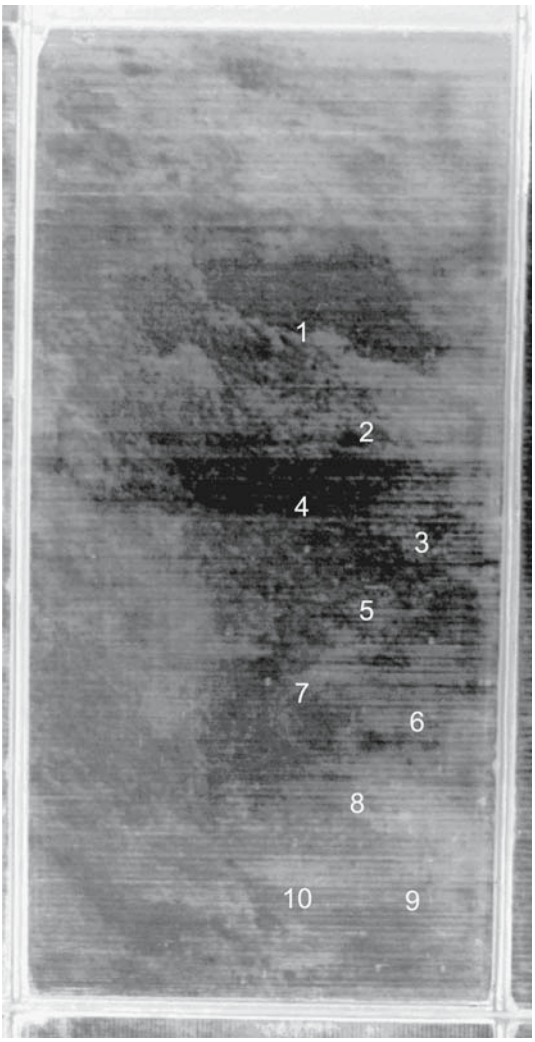


**Fig. 3** Near-infrared image of the 1,600 m × 800 m EBEX field site, with the tower site locations (1–10) indicated. This image is uncalibrated, however pyrgeometer measurements showed that the surface at sites 2 and 6 was approximately 4 K warmer than at sites 1, 4, and 5. The canopy was completely closed near sites 1–5. Sites 9 and 10 were in a less productive part of the field, where the canopy never completely closed. North is almost up (aligned with roads) in this image

$$R_{net} = R_{sw}\downarrow - R_{sw}\uparrow + R_{lw}\downarrow - R_{lw}\uparrow \tag{2}$$

where $R_{sw}$ is radiation in the shortwave (visible) and $R_{lw}$ the radiation in the longwave (infrared) portion of the spectrum measured over hemispheres representing both incoming to (↓) and outgoing from (↑) the surface.

The pyrgeometer data were processed using

$$R_{lw} = R_{pile} + \sigma T_{case}^4 + B\sigma \left(T_{dome}^4 - T_{case}^4\right) + fR_{sw} \tag{3}$$

where $R_{pile}$ is the output from the radiometer thermopile, $T_{case}$ and $T_{dome}$ are the temperatures of the radiometer case and dome, and $R_{sw}$ is the shortwave radiation incident on the dome, which is either incoming or outgoing, as with $R_{lw}$. The calibration of $R_{pile}$ and the determination of $B$ was done either at the World Radiation Center (WRC) in Davos, Switzerland or the National Oceanic and Atmospheric

**Table 2** Turbulence measurements at the EBEX sites

| Parameter | Sites 1,3 | Sites 2,4–6 | Site 7 | Site 8 | Site 9 |
|---|---|---|---|---|---|
| Wind velocity and $t_c$ | UW (4.7) | ATI-K (4.7) | ATI-K (4.7)<br>Kaijo-Denki TR90-AH (1.76)<br>Kaijo-Denki TR90-AH (2.7)<br>CSAT3 (2.7)<br>CSAT3 (4.7)<br>CSAT3 (8.7)<br>Metek USA-1 (4.7) | UW (4.7) | UW (4.7)<br>CSAT3 (2.4)×2<br>Gill R2 (2.4)<br>CSAT3 (6.0)<br>Gill HS (6.0)<br>Metek USA-1 (6.0) |
| Humidity | KH20 (4.7) | KH20 (4.7) | KH20 (4.7)×2<br>KH20 1.76<br>KH20 (2.7)×2<br>Li7500 (4.7)<br>KH20 (8.7) | KH20 (4.7) | KH20 (4.7)<br>KH20 (2.4)<br>KH20 (6.0)<br>Li7500 (6.0) |
| Fine-wire T | | | AIR150 (4.7)<br>Campbell (1.76)<br>Campbell (2.7)×2<br>Campbell (8.7) | | Heimann (6.0)×2 |

Heights in m above ground are in parentheses. Two sensors at one height are indicated by ×2

**Table 3** As for Table 1 for the profile measurements at the EBEX sites

| Parameter | Site 7 | Site 8 | Site 9 |
|---|---|---|---|
| Wind speed | Climatronics F460 (1.2,1.7,2.7,3.7,4.7,5.7×2, 6.7,7.7,8.7,9.7,10.7) | Modified RM Young (1.7,2.7,4.7,6.7,8.7,10.7) | Vector A101L (0.95,1.50,2.35,3.72,6.12,9.05) |
| Wind direction | Climatronics F460 (10.7) | Modified RM Young (1.7,2.7,4.7,6.7,8.7,10.7) | Vector W200P (9.0) |
| Temperature and humidity | Frankenberger (0.7,1.2,1.7,2.7,3.7,4.7,5.7, 6.7,7.7,8.7,9.7,10.7)<br>Vaisala HMP223 (2.47) | NCAR/Vaisala 50Y (0.7,1.7,2.7,4.7,6.7,8.7,10.2) | Frankenberger (0.95,1.50,2.35,3.72,6.12,9.05) |

**Table 4** The soil sensors used at the EBEX sites

| Parameter | Sites 1–6 | Site 7 | Site 8 | Site 9 |
|---|---|---|---|---|
| $T_{soil}$ | REBS (10–40) | REBS (10–40)<br>Pt100 (20,50,100,200,500) | REBS (10–40) | REBS (10–40)<br>CS107×4 |
| $Q_{soil}$ | CS615 (25) | CS615 (25) | CS615 (25) | CS615 (25) |
| $G_{soil}$ | REBS (50) | REBS (50)×2 | REBS (50) | REBS (50)<br>Rimco ×4 |

Depths (in mm) of the sensors are in parentheses. Two or four sensors at the same depth are indicated by ×2, ×4, respectively

Administration (NOAA) Climate Monitoring and Diagnostics Laboratory (CMDL) in Boulder, Colorado. The calibrations of $T_{dome}$ and $T_{case}$ were performed by the various research groups and $f$ was determined from in-field shading tests either during or after the experiment (see Kohsiek et al. 2007). In some cases, the value of $B$ was modified based on these shading tests.

**Table 5** The radiometers used to measure the radiation components

| Parameter | Sites 1–6 | Site 7 | Site 8 | Site 9 |
|---|---|---|---|---|
| $R_{net}$ | Q7 | Q7<br>CNR1<br>Schulze-Däke | Q7 | Q7<br>CNR1 |
| $R_{sw}\downarrow$ | | PSP<br>CM21v<br>CM14v | PSPv | PSP<br>CM21×2 |
| $R_{sw}\uparrow$ | PSP<br>CM21v | PSP<br>CM14v | PSPv | PSP<br>CM11 |
| $R_{lw}\downarrow$ | | PIRv | PIRv | PIR |
| $R_{lw}\uparrow$ | PIRv | PIRv | PIRv | PIR |
| $T_{sfc}$ | | KT15 | Everest ×4 | |

CM21, CM14, CNR1 are models by Kipp and Zonen, PIR and PSP are by Eppley, Q7 is by REBS. A "v" suffix indicates that the sensor was ventillated. All sensors were mounted on stands approximately 2 m above the ground. Two or four sensors at one position are indicated by ×2, ×4, respectively

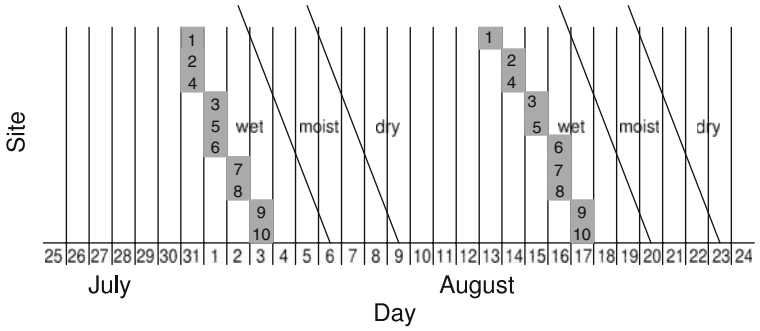


**Fig. 4** Schedule showing when each site was affected by irrigation during EBEX-2000. Shading indicates when there was standing water in the field. Note that the sites are ordered by their north to south position, rather than numerically

Since we expected clear skies, we chose to measure incoming radiation at only three sites and use most of our radiometers to determine the outgoing radiation at each tower site. All of these sensors were deployed on stands approximately 2 m above the ground (approximately 1 m above the top of the canopy) to have a field of view (for the downward-looking sensors) integrating over several rows of cotton plants. Table 5 shows the radiometer configuration that was used. Since redundant sensors often were available to measure the terms in Eq. (2), we follow the suggestion of Kohsiek et al. (2007) to use sensors with the best manufacturer's specification (generally Kipp & Zonen pyranometers and Eppley pyrgeometers for this study) and those sensors expected to have been the cleanest (either from manual cleaning or ventilation).

### 4.2 Sensible and latent heat fluxes

The sensible and latent fluxes are computed from

$$H = \rho_a c_p \overline{w'T'}, \tag{4}$$

$$LE = \rho_d l \overline{w'm_r'}, \tag{5}$$

where $\rho_a$ is the density and $c_p$ the specific heat of air, $\rho_d$ is the density of dry air, $l$ is the latent heat of vaporization of water, and $w'$, $T'$, and $m_r'$ are fluctuations of the vertical velocity, temperature, and water vapour mixing ratio, respectively. Unfortunately, in most cases, neither $\overline{w'T'}$ nor $\overline{w'm_r'}$ is measured directly. Thus, corrections to the measurements are needed.

All the fluxes described here were measured using a sonic anemometer and krypton hygrometer. (A few fast-response fine-wire temperature sensors and infrared hygrometers also were available during EBEX.) For this sensor combination, several processing steps must be applied in order to obtain sensible and latent heat fluxes. These are:

- Correction of the sonic temperature, derived from the speed of sound, for the effect of moisture.
- Correction of the krypton hygrometer data for absorption of ultraviolet light by oxygen.
- Application of the Webb et al. (WPL) correction to the water vapour flux.
- Correction for spatial separation between the sonic anemometer and krypton hygrometers.

Some groups participating in EBEX applied these steps iteratively and in different sequences. The data shown here were obtained by solving all of these equations analytically so no iteration was necessary. The differences between these procedures were found to be small for EBEX (Mauder et al. 2007) and the effect of interation negligible for the LITFASS-2003 experiment (Mauder et al. 2006).

In addition, sonic anemometers all require a cross-wind correction to their measured virtual temperature (e.g. Liu et al. 2001). The ATI, CSAT, and Gill anemometers applied this correction internally. For the Kaijo-Denki, UW, and METEK USA-1 we applied this correction in post-processing.

There also is filtering of the high-frequency part of both fluxes due to the spatial averaging along the physical path sampled by both the sonic anemometers and hygrometers and due to the temporal sampling. A complete treatment of these effects is beyond the scope of this study, however a rough estimate can be made from the expression of Horst (1997) using the time constant for sonic anemometer line averaging quoted by Massman (2000). The anemometers used in the following analysis had vertical pathlengths of about 0.15 m and were sampled at 10 or 20 samples $s^{-1}$. For a mid-day wind speed of nominally 2.5 m $s^{-1}$, this attenuation would be expected to be less than 2% and has been neglected.

It has been suggested by Gash and Dolman (2003) that systematic flux errors may occur if the instantaneous wind vector is outside the acceptance angle for the sonic anemometers that are used. For the relative smooth surface of EBEX (roughness length about 15 mm), daytime angles of attack were between –20 and +30° 99% of the time, which is well within the acceptable operating range of at least most of the anemometers used during EBEX (including the UW and ATI, whose data are shown below). More discussion of differences between the types of anemometers used during EBEX can be found in Mauder et al. (2007).

The next step was a change of the coordinate system so that the mean vertical wind is zero over the measuring period. We used a single rotation over the entire measurement period (Wilczak et al. 2001), which avoids many of the issues related to loss of energy at low frequencies discussed by Finnigan et al. (2003). Due to the flat terrain, the rotation angles were no more than two degrees, which was typical for the

sensor mounts that were used. The data were not detrended (Lee et al. 2004; Finnigan et al. 2003).

All of the turbulence data had basic quality control checks applied. Although some groups applied tests such as those of Vickers and Mahrt (1997) and Foken and Wichura (1996), updated by Foken et al. (2004), the quality control for the results presented here consisted primarily of outlier detection, including use of the algorithm of Højstrup (1993).

### *4.2.1 Sonic temperature*

The sonic (speed of sound) temperature is $t_c = T(1 + 0.51Q)$, where $T$ is absolute temperature and $Q$ is specific humidity (Kaimal and Gaynor 1991; Schotanus et al. 1983). Thus

$$\begin{aligned}\overline{w't'} &= \overline{w'T'_c} - 0.51T\overline{w'q'} \\ &\simeq \overline{w't'_c}/(1 + 0.06/B)\end{aligned} \tag{6}$$

where $B = H/LE$ is the Bowen ratio. Note that the specific humidity flux correction to $\overline{w't'_c}$ is important for $|B| < 1$ or $|H| < |LE|$, as was the case during EBEX. This equation was not needed when a fast response thermometer was available and $\overline{w'T'}$ can be calculated directly.

### *4.2.2 Oxygen correction*

The krypton hygrometer, KH2O, measures the absorption of ultraviolet radiation by both water vapour and oxygen. In order to obtain the water vapour density, the KH2O measurements must be corrected for absorption by oxygen (Tanner et al. 1993),

$$\rho_v = \rho_{vk} - \left(\frac{k_o}{k_w}\right)\frac{C_o M_o}{M_a}\rho_d \tag{7}$$

where $\rho_v$ is the actual water vapour density, $\rho_{vk}$ is the calibrated output of the KH20, $k_o$ and $k_w$ are the KH2O extinction coefficients for oxygen and water vapour, $C_o = 0.21$ is the percent concentration of oxygen in the atmosphere, $M_o = 32$ and $M_a = 28.97$ are the molecular weights of oxygen and dry air, and $\rho_d$ is the density of dry air. Van Dijk et al. (2003) have shown that $k_o$ depends on the pathlength of the krypton hygrometer. Their Table 2 provides the value of 0.00034 $\mathrm{m^3\,g^{-1}\,mm^{-1}}$ for the pathlength of 13 mm that was used during EBEX.

Ignoring the contribution of pressure fluctuations to $\rho'_d$,

$$\begin{aligned}\overline{w'\rho'_v} &= \overline{w'\rho'_{vk}} + C_{ko}(\rho_d/T)\overline{w'T'} \\ &\simeq \overline{w'\rho'_{vk}}/(1 - 8C_{ko}B)\end{aligned} \tag{8}$$

where

$$C_{ko} = \left(\frac{k_o}{k_w}\right)\frac{C_o M_o}{M_a} = 0.23\frac{k_o}{k_w}. \tag{9}$$

For the krypton hygrometer, $k_o/k_w$ is on the order of 1–2%, so that $C_{ko}$ is on the order of 0.5% or less. Thus the oxygen correction to $\overline{w'\rho'_{vk}}$ is important for $|B| > 1$ or $|H| > |LE|$, and thus was usually small for EBEX.

*4.2.3 WPL correction*

With correction for oxygen absorption, the kyrpton hygrometer measures water vapour density $\rho_v$. However, Webb et al. (1980) (WPL) show that the vertical flux of water vapour density is not equal to $\overline{w'\rho_v'}$, but rather

$$\begin{aligned}\frac{LE}{l} &= \rho_d \overline{w'm_r'} \\ &= \rho_a \overline{w'q'}/(1-Q) \\ &= (1+\mu M_R)[\overline{w'\rho_v'} + (\rho_v/T)\overline{w'T'}] \\ &\simeq (1+\mu M_R)\overline{w'\rho_v'}(1+8QB) \end{aligned} \tag{10}$$

where $M_R$ is the mean value of mixing ratio, $Q$ and $q'$ are the mean value and fluctuations of specific humidity, and $\mu = M_a/M_w$ =1/0.622 is the ratio of the molecular weights of dry air and water vapour. (See also Fuehrer and Friehe 2002; Leuning 2004.) Thus, the WPL correction is important only for $|B| > 1$ or $|H| > |LE|$ (again, not usually the case during EBEX) or for large values of $Q$ (which sometimes did occur). The effect of this correction was investigated for site 7 during EBEX by Liebethal and Foken (2003, 2004). We note that an alternative expression for this correction derived by Liu (2005) gives latent heat fluxes 1% lower than those using WPL for the EBEX dataset.

*4.2.4 Spatial separation*

In order to reduce flow distortion, the krypton hygrometer was displaced spatially from the sonic anemometer. This displacement reduces the correlation between the measurements of vertical velocity and scalar concentration. Kristensen et al. (1997) found that the corresponding reduction of the measured flux is minimized if the scalar sensor is placed below the anemometer. However, Wyngaard (1988) showed that "cross talk" error caused by flow distortion is eliminated if the sensor configuration has reflection symmetry about a horizontal plane through the measuring point, which requires a horizontal displacement of the scalar sensor.

Moore (1986) describes a correction for this displacement that assumes isotropy in the velocity and scalar fields. However, since isotropic turbulence cannot carry a flux, a similar correction based on the scalar cospectral function of Horst (1997) was used for most of our data. He assumed that the cospectrum has approximately the form

$$fCo(f) = \overline{w'\rho_v'}(2/\pi)(f/f_m)/[1+(f/f_m)^2] \tag{11}$$

where $f$ is frequency and $f_m$ is the frequency at the peak of the frequency-multiplied cospectrum. With this assumption, the correction for flux attenuation is (Horst 2003)

$$\begin{aligned} A &= \exp(2\pi f_m S/U) \\ &= \exp(2\pi n_m S/z) \end{aligned} \tag{12}$$

where $S$ is the sensor displacement, $U$ is mean wind speed, $n_m = f_m z/U$, and $z$ is the measurement height. Equation (12) provides a reasonable fit to the data of Kristensen et al. (1997), Fig. 5, for scalar flux attenuation due to horizontal sensor displacement. With the following formulae for $n_m$, it can be seen that the spatial separation correction is small for $S/z \ll 1$.

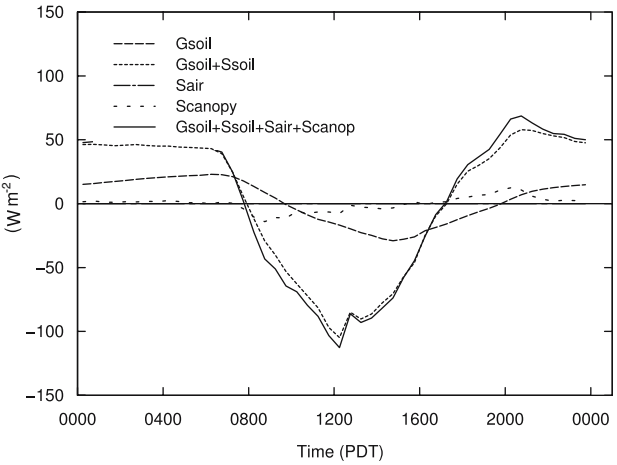


**Fig. 5** The diurnal composite over all sites and days of the total surface heating $G$ and the various terms comprising it. $G_{soil}$ is the heat flux measured by the heat flux plates at 50 mm depth, $S_{soil}$ is the heat storage in the soil above the heat flux plate, $S_{canopy}$ is the heat storage by the above-ground plant biomass, and $S_{air}$ is the heat storage by air in the canopy. Note that $S_{air}$ is undistinguishable from the reference line at 0

Fitting data from the Horizontal Array Turbulence Study (Horst et al. 2004) resulted in the following empirical relations for $n_{mx}$ and $n_{my}$, the values of $n_m$ in the streamwise and crosswind directions, respectively,

$$n_{mx} = \begin{cases} 0.065 & z/L < -0.1 \\ 2.16 - 2.095/(1.015 + 0.15z/L)^2 & z/L > -0.1 \end{cases} \tag{13}$$

and

$$n_{my} = \begin{cases} 0.15 & z/L < -0.05 \\ 2.43 - 2.28/(1.01 + 0.2z/L)^2 & z/L > -0.05 \end{cases} \tag{14}$$

(T. Horst, 2006, personal communication) where $L_0$ is the Obukhov length. As might be expected, $n_{my} > n_{mx}$ due to the stretching of eddies by vertical shear in the streamwise direction.

Using the suggestion of Lee and Black (1994) for the dependence of $n_m$ on wind direction,

$$n_m^2 = [n_{mx} \cos\alpha]^2 + [n_{my} \sin\alpha]^2 \tag{15}$$

where $\alpha$ is the wind direction relative to the direction of sensor separation ($\alpha = 0$ for wind direction parallel to sensor separation, and 90 degrees for wind direction normal to sensor separation). Lee and Black base this formula on the assumption of an elliptical shape for the turbulent eddies in the horizontal plane and show that it is consistent with their dataset for unstable stratification (Horst 2003).

### *4.2.5 Combined calculation*

Solving the above set of equations for $\overline{w'T'}$ and $\overline{w'm'_r}$ produces

$$\overline{w'T'} = [\overline{w't'_c} - C_{tc}(T/\rho_a)A\overline{w'\rho'_{vk}}]/[1 + C_{tc}(Q + C_{ko}(1 - Q))], \tag{16}$$

$$\overline{w'mr'} = (1 + \mu M_R)[(A/\rho_d)\overline{w'\rho'_{vk}} + ((C_{ko} + M_R)/T)\overline{w't'_c}]/[1 + C_{tc}(Q + C_{ko}(1 - Q))] \tag{17}$$

where $C_{tc} = 0.51[1 + Q(\mu - 1)]$ (T. Horst, 2003, personal communication).

*4.2.6 Averaging time*

The analysis that follows was processed using block averages of 30 min. Some recent work (e.g. Finnigan et al. 2003) has suggested that this averaging period may miss temporal scales that contribute to the flux. An ogive analysis (e.g. Oncley et al. 1996) on our data showed that, on average, including scales as long as 4 h contributes less than 5 W m$^{-2}$ (maximum pre-dawn) to $H$ and less than 10 W m$^{-2}$ (mostly a loss at night) to $LE$. Since averaging over several hours might obscure some of the processes that we are interested in, we have chosen not to use a longer period.

*4.2.7 Impact*

The effects of all these corrections were evaluated for a representative subset of the EBEX dataset.

- The WPL and spatial separation corrections have a clear diurnal variation with maxima in the early afternoon (local time).
- For daytime conditions, the spatial separation correction typically increases the latent heat flux by 7% and decreases the sensible heat flux by 2% (due to the increase in $\overline{w'q'}$ in Eq. 6). Sensor separation is the largest of these corrections.
- The WPL correction increases the latent heat flux by 2%.
- The sense of the WPL and spatial separation corrections is to reduce the energy balance residum.

4.3 Surface heat flux

To evaluate a surface energy balance, we need to choose a reference surface. We chose the top of the canopy $h_c$, since each of the energy balance terms can be readily evaluated there. Thus, the surface heat flux $G$ must take into account all the heat transfer below the canopy top. We divide this heating into the heat storage by plant and air mass within the canopy $S_{canopy}$ plus the heat flux at the top of the soil $G(0)$. In turn, $G(0)$ is determined from measurements by heat flux plates at a depth $z_p$ and the heat stored by the soil between the surface and $z_p$. Thus

$$G(h_c) = S_{canopy} + S_{soil} + G(z_p). \tag{18}$$

The sampling in time and space of these terms were (necessarily) not the same, and so we adopted an approach of creating a composite average for the entire EBEX site based on the data that were available.

*4.3.1 Soil heat flux*

$G(z_p)$ was measured at sites 1–9 using REBS heat flux plates (HFT) at a depth $z_p$ of 50 mm. The Philip (1961) correction for these plates is of the form (his Eq. 8):

$$f(\epsilon) = \frac{G_p}{G_s} = \frac{1}{1 - 1.92\frac{X_p}{D}(1 - \lambda_s/\lambda_p)} \tag{19}$$

where $G_p$ and $G_s$ are the heat fluxes through the plate and through the soil, $X_p = 3.93\,\mathrm{mm}$ is the plate thickness, $D = 38.56\,\mathrm{mm}$ is the plate diameter, and $\lambda_p = 1.22\,\mathrm{W\,m^{-1}\,K^{-1}}$ and $\lambda_s$ are the thermal conductivities of the plate and soil, respectively. Our plates were calibrated by the manufacturer in a water/glass bead medium with thermal conductivity $\lambda_m = 0.906\,\mathrm{W\,m^{-1}\,K^{-1}}$ and gave a measured value $G_m$ based on this calibration coefficient. Thus, for our plates

$$G_s = \frac{G_p}{f(\lambda_p/\lambda_s)} = \frac{G_m f(\lambda_p/\lambda_m)}{f(\lambda_p/\lambda_s)} = \frac{1.053 G_m}{f(\lambda_p/\lambda_s)}. \tag{20}$$

During the field campaign a small sample of soil was saved, and in the laboratory a Hukseflux TP01 probe was embedded in this sample to determine $\lambda_d = 0.18\,\mathrm{W\,m^{-1}\,K^{-1}}$, when dry. For moist soil, we expect

$$\lambda_s = Q_{soil}\lambda_w + (1 - Q_{soil})\lambda_d, \tag{21}$$

where $\lambda_w = 0.6\,\mathrm{W\,m^{-1}\,K^{-1}}$ is the thermal conductivity of water and $Q_{soil}$ is the volumetric soil moisture fraction, which ranged from 5 to 60% during the experiment. For these values $f(\lambda_p/\lambda_c)/f(\lambda_p/\lambda_s) = 0.88$–$0.92$. Thus, our measured soil heat flux would be about 10% low. This correction has been applied to the data, though some variability in $\lambda_d$ across the field is expected.

### *4.3.2 Soil heat storage*

Next, we need to calculate the heat storage in the soil above $z_p$,

$$S_{soil} = -c_{soil} z_p \frac{dT_{soil}}{dt} \tag{22}$$

where

$$c_{soil} = \rho_{water} Q_{soil} c_{water} + \rho_{soil.dry} c_{soil.dry}. \tag{23}$$

and $T_{soil}$ is the soil temperature. Laboratory measurements of our one soil sample found $c_{soil.dry} = 2900\,\mathrm{J\,(K\,kg)^{-1}}$.

$T_{soil}$ was measured using a REBS linear soil temperature probe at each site, positioned to average between 10 and 40 mm. Since we expect the soil temperature to vary most at the top of the soil, $dT_{soil}/dt$ probably is slightly underestimated by not having a measurement in the 0–10 mm layer of soil. We have no means of estimating this magnitude. The temperature at site 7 was seen to vary significantly more than at the other sites, probably due to a probe that was directly exposed to the air by cracking of the soil. Thus this site was not included in the composite.

$Q_{soil}$ was also measured at sites 1–9 using Campbell Scientific, Inc. CS615 soil moisture probes set at 50 mm depth. We calibrated the $Q_{soil}$ measurements based on gravimetric measurements that were made 2–9 times during the experiment (depending on the site). The probes at sites 1 and 2 were faulty (site 1 was replaced on 12 August), so the average of all the gravimetric measurements at each site was substituted for these missing data.

*4.3.3 Canopy heat storage*

The heating of the canopy has contributions from both the plant material and the air between the plants

$$S_{canopy} = S_{plant} + S_{air}. \tag{24}$$

We made independent measurements of leaves and stems, so the plant storage term is further divided into

$$S_{plant} = S_{leaf} + S_{stem}. \tag{25}$$

To form the composite for EBEX, both $S_{leaf}$ and $S_{stem}$ are averages using temperature measurements from two sites. We deployed a total of 28 thermocouples in leaves and another 20 thermocouples in plant stems at site 10 and at another location near site 9. On average, the leaf and stem temperatures were quite similar. However, large temporal changes were observed due to the variation of illumination caused by the shading of particular plant elements within the canopy. The observations were grouped by height within the canopy in four height ranges: 0–0.2, 0.2–0.4, 0.4–0.6, and 0.6–0.8 m. Canopy mass (also height-grouped) was further separated into water and cellulose (where all plant matter is taken to be cellulose, including flowers and cotton) that were derived from destructive canopy biomass samples. Biomass values were linearly interpolated in time from samples taken on two days (3 and 21 August) at two sites—site 10 and another location near the north-east corner of the EBEX field.

Storage of heat in the air between the plants is calculated as:

$$S_{air} = h_c \left[ \rho_{air} c_p \frac{dT}{dt} + L(T) \frac{d\rho_v}{dt} \right], \tag{26}$$

which includes the storage of sensible heat of the moist air and of latent heat. In this equation,

$$c_p = c_{pd}(1 + 0.84Q) \tag{27}$$

and

$$L(T) = 2.501 \times 10^6 - 2361T \tag{28}$$

(Shuttleworth 1993) with $T$ in kelvin and the heat capacity of dry air $c_{pd} = 1,006\,\mathrm{J\,K^{-1}\,kg^{-1}}$. We used 1 m as the average canopy height $h_c$ over the EBEX field for this composite and $T$ and $Q$ were determined from measurements by one hygrothermometer deployed at 0.7 m (within the canopy) at site 8.

Figure 5 shows the contributions of each of these sub-terms to $G(h_c)$. Even at only 50 mm depth, $G(z_p)$ is relatively small, with a daytime maximum of only $30\,\mathrm{W\,m^{-2}}$. At the same time, $S_{soil}$ has a maximum value of over $100\,\mathrm{W\,m^{-2}}$, implying that the most important measurement contributing to our estimate of $G(h_c)$ is simply $T_{soil}$ and that it is critical to obtain a reliable value for $C_{soil}$. On short time scales (not shown) individual measurements of $S_{plant}$ had large variations since parts of the plants were progressively illuminated by direct sunlight and then shaded. However, on average, $S_{plant}$ contributed a relatively small maximum of $10\,\mathrm{W\,m^{-2}}$. Because $T_{air}$ never experienced rapid changes, $S_{air}$ is negligible.

## 5 Energy budget

We now can produce a total energy budget for EBEX. Figure 6 presents a diurnal composite over the entire operations phase of the experiment for all stations. The lack of clouds causes $R_{net}$ to follow nearly ideal cosine behaviour. Also, EBEX clearly achieved the goal of measuring large latent heat fluxes, with midday values about (2/3) $R_{net}$. Indeed, with the large transpiration, sensible heat fluxes became negative (stable stratification) in mid-afternoon—an "oasis effect", with this mid-afternoon change in the sign of the sensible heat flux consistent with changes seen in the air temperature profiles.

The magnitude of $G$ is larger than $H$ and even the magnitude of $S_{soil}$ is usually larger than $H$. This means that a single soil temperature measurement at each site had a larger effect on our measurement of the diurnal variation of the energy balance than the eddy-covariance measurement of sensible heat.

Figure 6 shows that there is close to an energy balance at night, with a "double-balance" of $G \approx R_{net}$ and $H \approx -LE$. However, during the day, the midday imbalance is 70 W m$^{-2}$ or 10% of $R_{net}$.

To investigate this imbalance, we examine the spatial variability of the major terms. Figure 7 shows the differences in $R_{net}$ between the sites. As also shown by Kohsiek et al. (2007), the total variability is only on the order of 30 W m$^{-2}$ though the point-to-point differences were larger by about a factor of 3. Part of this variability might be due to slight mislevelling of the sensors. We conclude that the spatial variability of the radiative fluxes was not large, despite the differences in the surface apparent in Fig. 3.

Figure 8 shows the major term balance for each site. The overall pattern is quite similar for all sites, though there are differences. Site 7 is unique in having a balance in the morning and site 6 is remarkable in actually having a negative imbalance (the sum of the other terms larger than $R_{net}$) in the early afternoon. Although $R_{net}$ was quite similar at all of the sites, the other major budget terms have significant differences. Surface heating at sites 1, 2, and 4 are smaller than at the other sites. Latent heat flux

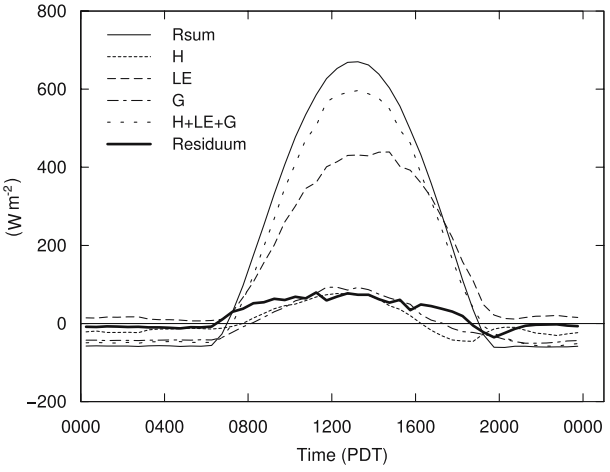


**Fig. 6** The diurnal composite of the surface energy balance for EBEX from all sites over the entire measurement period. Shown are the "Major Terms" described in Sect. 5

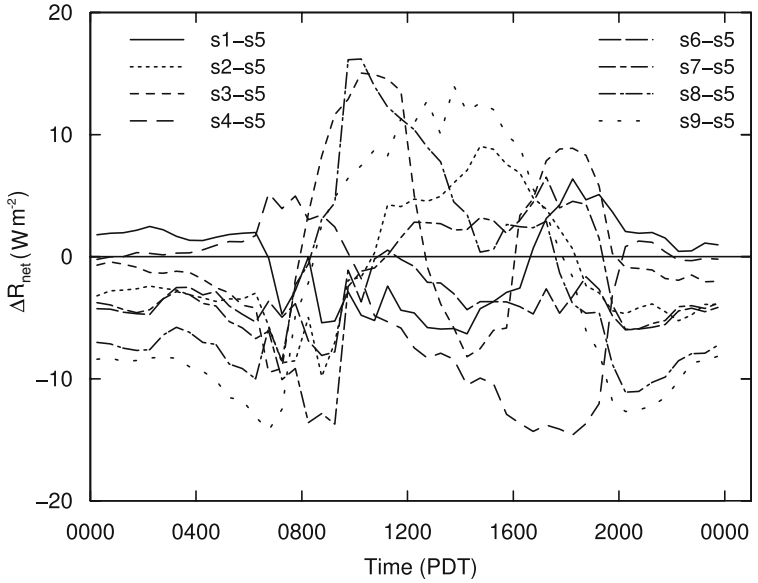


**Fig. 7** The diurnal composite of net radiation from each of the sites, referenced to site 5

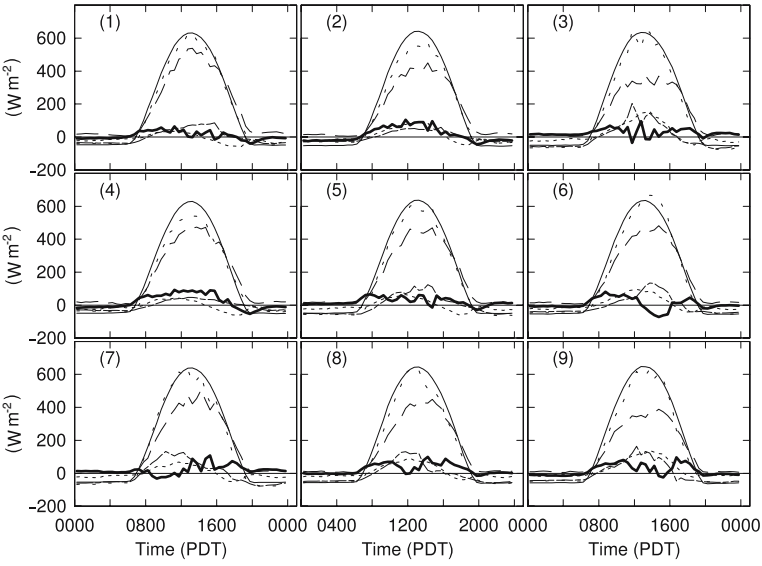


**Fig. 8** Same as Fig. 6, but for each site during EBEX

at site 1 is significantly larger than at the other sites, with values at sites 2, 3, and 9 almost appearing to be "clipped" at midday. Sensible heat flux has a suggestion of an east-west gradient, with sites 1, 4, and 7 generally lower than sites 3, 6, and 9. Most of these differences are consistent with the spatial variation of the canopy density and together explain the rather large site-to-site differences in, say, the magnitude of the

imbalance at midday. However, none of these effects explains the overall imbalance. Thus, we need to pursue other explanations.

## 6 Minor terms

The imbalance we observe obviously is caused by errors in the measurement of the above terms or there are additional terms that have not been included. Indeed, because the vegetation surface during EBEX was not uniform, it is possible for a vertical divergence of the flux to exist. We now investigate this divergence, along with two other terms in Eq. (1).

### 6.1 Vertical flux divergence/horizontal advection

A possible source of imbalance is vertical flux divergence, and that the flux we measure at 4.7 m is lower than the actual flux at the surface (canopy top) (Aubinet et al. 2003; Finnigan 2004). There are two ways to determine this loss; the actual measurement of the vertical flux profiles and the measurement of horizontal advection of heat in the layer from 4.7 m to the surface. These are related by writing the budgets for temperature and humidity in this layer

$$\frac{\partial \overline{T(z)}}{\partial t} + \overline{U_i(z)} \frac{\partial \overline{T(z)}}{\partial x_i} + \frac{\partial \overline{u_i' T'}}{\partial x_i} = 0 \tag{29}$$

and

$$\frac{\partial \overline{Q(z)}}{\partial t} + \overline{U_i(z)} \frac{\partial \overline{Q(z)}}{\partial x_i} + \frac{\partial \overline{u_i' q'}}{\partial x_i} = 0 \tag{30}$$

where we use the convention of summing over repeated indices in each term. Integrating Eq. (29) from the surface to the flux measurement height $z_m$ and solving for the vertical flux at the surface yields

$$\begin{aligned} \overline{w'T'}_{h_c} - \overline{w'T'}_{z_m} = & \int_{h_c}^{z_m} \frac{\partial \overline{T(z_m)}}{\partial t} dz + \int_{h_c}^{z_m} \overline{U(z)} \frac{\partial \overline{T(z)}}{\partial x} dz + \int_{h_c}^{z_m} \overline{V(z)} \frac{\partial \overline{T(z)}}{\partial y} dz \\ & + \int_{h_c}^{z_m} \frac{\partial \overline{u'T'}(z)}{\partial x} dz + \int_{h_c}^{z_m} \frac{\partial \overline{v'T'}(z)}{\partial y} dz \end{aligned} \tag{31}$$

where $\overline{W(z)}$, $\overline{U(h_c)}$, and $\overline{V(h_c)}$ are assumed to be negligible. Since vertical profiles were only measured at sites 7, 8, and 9 (which were colinear), and fluxes were mostly measured only at $z_m = 4.7$ m, Eq. (31) was evaluated as

$$\begin{aligned} \overline{w'T'}_{h_c} - \overline{w'T'}_{z_m} = & \; z_m \frac{\partial \overline{T(z_T)}}{\partial t} + z_m \overline{U(z_u)} \frac{\partial \overline{T(z_T)}}{\partial x} + z_m \overline{V(z_u)} \frac{\partial \overline{T(z_T)}}{\partial y} \\ & + z_m \frac{\partial \overline{u'T'}(z_m)}{\partial x} + z_m \frac{\partial \overline{v'T'}(z_m)}{\partial y} \end{aligned} \tag{32}$$

where $z_u$ is 2.7 m and $z_T$ is 2.0 m to best represent the average values within the $h_c$ to $z_m$ layer, given the measurements that were made. A similar equation was used for humidity. Summing all of the terms on the right-hand side produces the dashed line in Fig. 9. Mean horizontal advection of humidity is the largest of all of the terms in

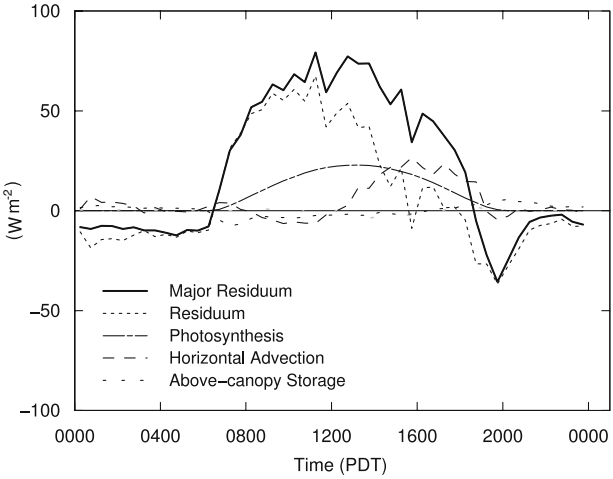


**Fig. 9** The diurnal composite of the minor surface energy balance terms, along with the residuum found from the major terms for EBEX from all sites over the entire measurement period

Eq. (32) and has a maximum value in the afternoon, due to a build-up of moisture close to the surface in the most productive section of the field. All of the other terms have a magnitude less than 5 W m$^{-2}$.

An alternative method to determine the vertical flux divergence is from direct measurements. Clearly, we could not measure exactly at the surface, due to the inability of finite-sized sonic anemometers to capture the smaller turbulence scales near the surface. However, the gradient may be estimated from observations at different heights. We measured sensible and latent heat fluxes at 1.76, 2.7, 4.7, and 8.7 m at site 7 and at 2.4, 4.7 and 6 m at site 9.

At site 7, the lowest measurements were made by Kaijo-Denki sonic anemometers with a 50-mm pathlength each with a colocated krypton hygrometer. Distortion of the air flow by the (necessarily closely colocated) hygrometer was significant. However, a correction of 13% was found by comparison to the CSAT3 anemometer also at 2.7 m at this site (Mauder et al. 2007). Thus, the flux gradients were estimated from the difference between the Kaijo-Denki anemometers at 1.76 and 2.7 m.

At site 9, the flux gradients were estimated from measurements made by two Gill anemometers—an R2-style array at 2.4 m and an HS-style at 6.0 m, each with colocated krypton hygrometers. As noted earlier, the fluxes at this site were somewhat different due to the thinner vegetation and probably are not representative of the overall EBEX site.

Figure 10 shows the vertical gradient of the sensible heat flux estimated from these measurements, normalized to the height difference of 4 m between the surface and our standard flux measurements. The mean horizontal advection calculated above and the energy balance residuum from the major terms also are shown. The magnitudes of these terms are small, but agree with the mean advection. The site 9 values are generally smaller than those at site 7, which is somewhat surprising given the larger sensible heat fluxes there. Presumably, the area with a thinner canopy was large enough to include the flux footprints for measurements at both 2.4 and 6.0 m.

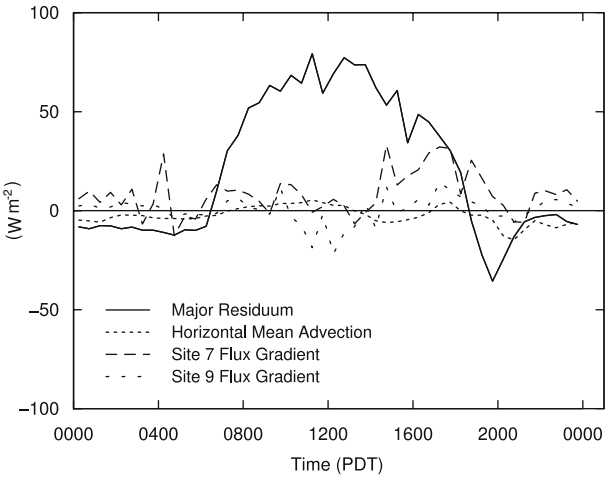


**Fig. 10** The diurnal composite of the mean horizontal advection of sensible heat along with the vertical sensible heat flux divergence calculated from direct measurements at sites 7 and 9. The residuum found from the major terms is shown for comparison. Positive values indicate heat accumulating near the surface

**Fig. 11** As Fig. 10 for latent heat flux

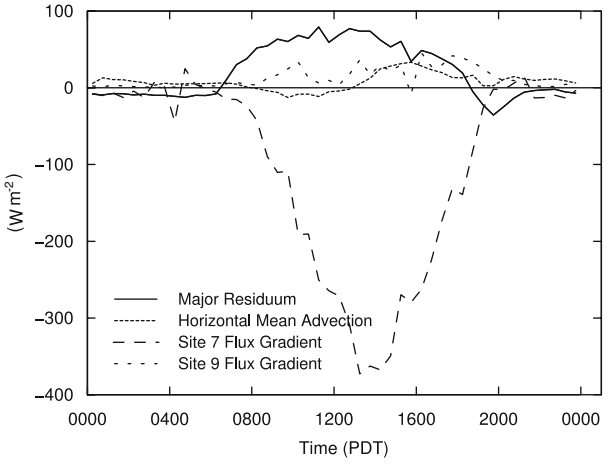


However, the latent heat fluxes shown in Fig. 11 clearly do not agree. The mean advection term shows latent heat leaving the layer below $z_m$ horizontally in the afternoon. The average flux gradient measurements from site 9 generally agree with this trend, although the daytime flux gradient changed sign during this period as the fetch shifted to include areas where the canopy density was higher than that of the local surface. The gradients from the Kaijo-Denki measurements at site 7 are dramatically different, with lower latent heat fluxes closer to the ground. (Actually, the difference in the magnitude of the fluxes between the lower and upper measurements was similar between sites 7 and 9 late in the experiment, but the different flux measurement heights cause the gradients to be a factor of 4 more at site 7.) Lower latent heat flux near the ground is in the opposite sense of what is usually assumed for flux gradients (largest fluxes near the source of humidity at the surface) and also opposite

to what would be needed to close the energy balance. Spatial filtering of the turbulence by the sonic anemometers is an obvious possible cause of this problem (none of the fluxes presented here have been corrected for this effect), but is expected to be small—especially for the Kaijo-Denki sensors with a 50-mm pathlength (Horst 1997). A change in vegetation density is another possible source of this reverse flux gradient. At site 9, this effect is likely (thinner vegetation near the measurement site), however the vegetation was relatively uniform near site 7.

### 6.2 Photosynthesis

The basic chemical equation that plants use to create glucose is

$$6H_2O + 6CO_2 \stackrel{h\nu}{\rightarrow} C_6H_{12}O_6 + 6O_2. \tag{33}$$

This process takes energy from the visible radiation spectrum (from 400 to 700 $\mu$m—photosynthetically active radiation, PAR) and converts it to chemical energy in glucose molecules. This is the gross primary productivity (GPP) of the plants. The glucose is both converted to plant material (e.g. cellulose) and consumed by the plants to give them energy. The net energy of these processes is the net primary productivity (NPP). Adding to this the consumption of organic material in the soil by microbes results in the net ecosystem exchange (NEE).

A value for GPP is needed to close the energy balance since the chemical energy released through plant and soil respiration presumably goes into heat that is part of the sensible heat flux or surface heating discussed above. However, we did not measure GPP. Thus, we determined NPP and NEE and use the "rule of thumb" that GPP is two and four times, respectively, these values.

We measured PAR at site 7. Using the value of radiation-use efficiency of 1.66 found for mature cotton by Milroy and Bange (2003), this energy becomes NPP. We find a peak value NPP of 12 W m$^{-2}$ with a diurnal average of 3.8 W m$^{-2}$ during EBEX. To check this value, a lower bound is the average value of NPP over the entire growing season. We measured total dry biomass from samples during the field campaign and also had available the total yield at the end of the growing season. Our samples had a median value for the above-ground biomass of 0.67 kg m$^{-2}$ and a total yield of 0.55 kg m$^{-2}$. Although taken later in the growing season, the total yield was estimated after application of a defoliant and probably does not include leaves. Assuming that about 46% of this mass is carbon, and estimating the growing season to be 4.5 months, the average energy flux would be 1.0 and 0.9 W m$^{-2}$, respectively for both estimates of NPP. Note that we have only accounted for above-ground biomass in this estimate. With the inclusion of below-ground biomass, these values would be about 25% higher (Derner et al. 2003), but clearly are lower than 3.8 W m$^{-2}$, as expected. The corresponding diurnal average value of GPP would be 7.6 W m$^{-2}$.

We also can convert our measurements of the flux of $CO_2$ (from sites 7 and 9) to NEE of the cotton. Since the energy to fix one mole of glucose is $2.86\times10^6$ J, NEE has a peak value of 12 W m$^{-2}$ and a diurnal average of 2.0 W m$^{-2}$. The corresponding diurnal average value of GPP would be 8.0 W m$^{-2}$, very close to our NPP-derived estimate.

Although there is some uncertainty in these values, they definitely are small compared to our energy balance closure (see Fig. 9). We have the most confidence in the

NEE estimate, however the PAR-derived estimate is shown in Fig. 10 since PAR (like GPP) never is negative.

### 6.3 Water pumping

Our final term is the mechanical work expended by plants to move water up from the soil to their leaves. Assuming that the average vertical motion is over the height of the canopy (the middle of the root zone to the middle of the canopy), this energy is $gh_c(LE/L) \approx 4 \times 10^{-6} LE$, which clearly is negligible. We note that this is not the thermal effect of water transfer described by Gao (2005), which we have already accounted for by including a moist heat capacity.

## 7 Discussion

### 7.1 Irrigation

The effect of irrigation was subtle during EBEX (see Fig. 12), consistent with the results of Oncley et al. (1993). The biggest effect was on the sensible heat flux, where the amplitude of the daytime maximum decreased and the amplitude of the nighttime minimum increased, both due to cooling of the surface. There is a corresponding increase in latent heat flux during irrigation, but the magnitude of this variation on both fluxes is only about $10\,\mathrm{W\,m^{-2}}$. Note that the effect of irrigation on both fluxes occurs about a day before the water reached the site, presumably because the irrigation was earlier applied upwind of the towers. Despite an observed change in albedo due to the darkening of moist leaves and changes in $R_{net}$ at specific sites, the composite $R_{net}$ over most sites showed no obvious difference through irrigation events. (An effect was seen at site 9 that had a less dense canopy, as described by Kohsiek

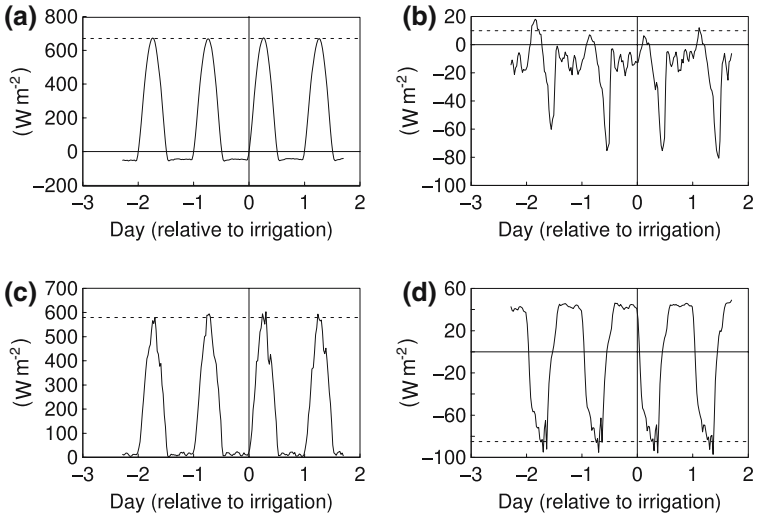


**Fig. 12** Composites over all sites of $R_{net}$ (**a**), $H$ (**b**), $LE$ (**c**), and $G$ (**d**) for two days before and after irrigation water reached each site. Dashed reference lines are shown to aid in detecting changes

et al. 2007.)Similarly, no effect is seen on $G$. Apparently, the wetter soil had smaller temperature changes which balanced the increase in heat capacity.

It has been suggested that liquid water advects heat from the surface during irrigation. EBEX did not include measurements of the water to determine the magnitude of this effect. However, the surface energy residuum appears to be unchanged by irrigation events, so we suspect that this effect is small.

### 7.2 Diurnal effects

While the net radiation and surface heating have a symmetric diurnal variation, the sensible and latent heat fluxes are asymmetric due to the oasis effect. It also appears that scalar similarity between $H$ and $LE$ breaks down to some extent as a function of the time of day. Using data from site 7, Ruppert et al. (2006) found by wavelet analysis that diurnal variations of the variance of sensible and latent heat fluxes are not similar for events longer than 40 s, except during the early afternoon. In the morning and late afternoon, sensible heat transfer is dominated by events with scales of 40–60 s, but latent heat transfer is dominated by scales longer than 100 s.

### 7.3 Soil macropores

As mentioned above, the clay soil at the EBEX site developed cracks during drying after irrigation. Less obvious macropores also may have developed in this soil. These openings could provide a direct pathway between layers of soil below our measurements of $G(z_p)$ and the atmosphere. In particular, evaporation of moisture below $z_p$ would contribute to our measurements of $LE$ using energy that had already been included in $G$. We have no way of quantifying this effect, though a crude upper limit is to multiply $G(z_p)$ by the ratio of the exposed surface area below $z(p)$ to that above $z_p$. Soil surface geometry was not measured during EBEX, but this ratio probably was less than 20%. Thus, the magnitude probably is below $10\,\mathrm{W\,m^{-2}}$. We note that the sense of this effect would be to increase the energy imbalance.

## 8 Conclusions

EBEX collected an excellent dataset for evaluating the surface energy balance. We have found that critical attention to calibration, maintenance, and software corrections of data from all sensors is essential to obtain hourly fluxes good to $10\,\mathrm{W\,m^{-2}}$. Despite this effort, the EBEX dataset still contains an imbalance on the order of 10% (the signed diurnal average) that we are unable to explain. Thus, we have attempted here to characterize the imbalance to assist in later explanations.

We are quite confident in our measurements of the major terms in the energy budget. Our radiation measurements all use the values from just one sensor each for incoming longwave and shortwave radiation, in part due to the amount of cleaning that was necessary. Our extensive surface heating measurements also depended heavily on simply one soil temperature sensor at each site, one air temperature and humidity sensor within the canopy, and one laboratory soil sample that was taken. We have no reason to doubt these individual measurements though we obviously cannot state how representative they were. The sensible heat fluxes were small, so most of our doubt lies in the latent heat flux observations, yet our intercomparison was able to

obtain reasonably good agreement between the instrument combinations that were used. Increasing the flux averaging time does not change the imbalance.

The nighttime energy budget closure was good, so most of the imbalance is during the day. The imbalance quickly grows to nearly its midday value, suggesting that the cause does not simply scale with any one of the energy terms. Our estimates of horizontal advection are roughly consistent with the vertical flux divergence measurements at site 9, indicating that at least part of the imbalance is due to non-local effects. This advection appears to explain the late afternoon imbalance, but not the imbalance earlier in the day. We observe "inverse" latent heat flux gradients that suggest that advection at small scales may be stronger than our field-scale observations indicate. Complicating the interpretation of all of our data are spatial inhomogeneities caused by the pattern of flood irrigation and (presumably) by variations in soil composition.

In hindsight, we can suggest several improvements for future observational energy budget studies. Temperature, humidity, and wind sensors within the canopy should be added to investigate sub-canopy drainage. We believe this drainage was small for our site simply due to flow obstruction by the leaves in the closed canopy (and thus a small advection velocity). We deployed a sodar, but profile measurements documenting the entire daytime boundary layer would have been useful. We made measurements in a horizontal plane at one height and a vertical plane in the along-wind direction, but a true three-dimensional mapping of wind, temperature, and humidity (with equal along- and cross-wind spacing) would have improved our estimates of horizontal advection. Finally, although we did deploy one station in an adjacent field, we lacked information about the upwind fluxes for all wind directions.

**Acknowledgements** Each participant in EBEX was funded primarily through his or her own institution and personal resources. Many support staff at each of these institutions also contributed to EBEX. Funding for the deployment of the NCAR Integrated Surface Flux Facility was provided by the National Science Foundation. Imagery of the EBEX site used in Fig. 3 was provided by Glenn Fitzgerald with the U.S. Department of Agriculture, Agricultural Research Service. Arrangements for use of the field site were facilitated by Bruce Roberts, Director of the University of California Cooperative Extension, Kings County. Westlake Farms generously provided both use of the land for this experiment and helped with logistical support. Thomas Horst (NCAR) contributed significantly to the sensor separation discussion. We are grateful to all of these people and organizations.

## References

Aubinet M, Grelle A, Ibrom A, Rannik Ü, Moncrieff J, Foken T, Kowalski AS, Martin PH, Berbigier P, Bernhofer C, Clement R, Elbers J, Granier A, Grünwald T, Morgenstern K, Pilegaard K, Rebmann C, Snijders W, Valentini R, Vesala T (2000) Estimates of the annual net carbon and water exchange of forests: the EUROFLUX methodology. Adv Ecol Res 30:113–175

Aubinet M, Heinesch B, Yernaux M (2003) Horizontal and vertical CO2 advection in a sloping forest. Boundary-Layer Meteorol 108:397–417

Beyrich F, Richter SH, Weisensee U, Kohsiek W, Lohse H, DeBruin HAR, Foken T, Göckede M, Berger FH, Vogt R, Batchvarova E (2002) Experimental determination of turbulent fluxes over the heterogeneous LITFASS area: selected results from the LITFASS-98 experiment. Theor Appl Climatol 73:19–34

Bolle H-J, Andr J-C, Arrie JL, Barth HK, Bessemoulin P, Brasa A, DeBruin HAR, Cruces J, Dugdale G, Engman ET, Evans DL, Fantechi R, Fiedler F, Van de Griend A, Imeson AC, Jochum A, Kabat P, Kratsch P, Lagouarde J-P, Langer I, Llamas R, Lopes-Baeza E, Melia Muralles J, Muniosguren LS, Nerry F, Noilhan J, Oliver HR, Roth R, Saatchi SS, Sanchez Diaz J, De Santa Olalla M, Shutleworth WJ, Sogaard H, Stricker H, Thornes J, Vauclin M, Wickland D (1993) EFEDA: European field experiment in a desertification-threatened area. Ann Geophys 11:173–189

Braud J, Noilhan P, Bessemoulin P, Mascart P, Haverkamp R, Vauclin M (1993) Bare ground surface heat and water exchanges under dry conditions. Boundary-Layer Meteorol 66:173–200
Culf AD, Foken T, Gash JHC (2004) The energy balance closure problem. In: Kabat P et al (eds.), Vegetation, water, humans and the climate. A new perspective on an interactive system. Springer, Berlin, pp 159–166
Derner JD, Johnson HB, Kimball BA, Pinter PJ Jr, Polley HW, Tischler CR, Boutton TW, Lamorte RL, Wall GW, Adam NR, Leavitt SW, Ottman MJ, Matthias AD, Brooks TJ (2003) Above- and below-ground responses of C3-C4 species mixtures to elevated CO2 and soil water availability. Global Change Biol 9:452–460
Elagina LG, Zubkovskii SL, Kaprov BM, Sokolov DY (1973) Experimental investigations of the energy balance near the surface (in Russian). Trudy GGO 296:38–45
Elagina LG, Kaprov BM, Timanovskii DF (1978) A characteristic of the surface air layer above snow. Izv Acad Sci USSR, Atmos Ocean Phys 14:926–931 (in Russian)
Finnigan J (2004) Advection and modeling. In: Lee X, Massman WJ, Law B (eds.), Handbook of micrometeorology: a guide for surface flux measurement and analysis. Kluwer Academic Publishers, Dordrecht, pp 209–244
Finnigan JJ, Clement R, Malhi Y, Leuning R, Cleugh H (2003) A re-evaluation of long-term flux measurement techniques part I: averaging and coordinate rotation. Boundary-Layer Meteorol 107:1–48
Foken T (1990) Turbulenter energieaustausch zwischen Atmosphäre und Unterlage - Methoden, messtechnische Realisierung sowie ihre Grenzen und Anwendungsmöglichkeiten. Ber Dt Wetterdienstes 180:287 pp
Foken T (1998) Die scheinbar ungeschlossene Energiebilanz am Erdboden - eine Herausforderung an die Experimentelle Meteorologie. Sitzungsberichte der Leibniz-Sozietät, ISSN 0947-5850, 24:131–150
Foken T (2003) Angewandte Meteorologie, Mikrometeorologische Methoden. Springer, Heidelberg, 289 pp
Foken T, Oncley S (1995) A report on the workshop: instrumental and methodical problems of land-surface flux measurements. Bull Amer Meteorol Soc 76:1191–1193
Foken T, Wichura B (1996) Tools for quality assessment of surface-based flux measurements. Agric Forest Meteorol 78:83–105
Foken T, Gerstmann W, Richter SH, Wichura B, Baum W, Ross J, Sulev M, Mölder M, Tsvang LR, Zubkovskii SL, Kukharets VP, Aliguseinov AK, Perepelkin VG, Zeleny J (1993) Study of the energy exchange processes over different types of surfaces during TARTEX-90'. Forschung und Entwicklung, Arbeitsergebnisse 4, Deutscher Wetterdienst, Offenbach am Main, ISSN 1430-0281, 34 pp
Foken T, Jegede OO, Weisensee U, Richter SH, Handorf D, Görsdorf U, Vogel G, Schubert U, Kirzel H-J, Thiermann V (1997) Results of the LINEX-96/2 experiment. Forschung und Entwicklung, Arbeitsergebnisse 48, Deutscher Wetterdienst, Offenbach am Main, 75 pp
Foken T, Göckede M, Mauder M, Mahrt L, Amiro BD, Munger JW (2004) Post-field data quality control. In: Lee X, Massman WJ, Law B (eds.), Handbook of micrometeorology: a guide for surface flux measurement and analysis. Kluwer Academic Publishers, Dordrecht, pp 181–208
Fuehrer PL, Friehe CA (2002) Flux correction revised. Boundary-Layer Meteorol 102:415–457
Gao Z (2005) Determination of soil heat flux in a Tibetan short-grass prairie. Boundary-Layer Meteorol 114:165–178
Gash JHC, Dolman AJ (2003) Sonic anemometer (co)sine response and flux measurement I. The potential for (co)sine error to affect sonic anemometer-based flux measurements. Agric Forest Meteorol 119:195–207
Herckes P, Lee T, Trenary L, Kang G, Chang H, Collett JL Jr (2002) Organic matter in central California radiation fogs. Environ Sci Technol 36:4777–4782
Højstrup J (1993) A statistical data screening procedure. Measuring Sci Technol 4:153–157
Horst TW (1997) A simple formula for attenuation of eddy fluxes measured with first-order response scalar sensors. Boundary-Layer Meteorol 82:219–233
Horst TW (2003) Attenuation of scalar fluxes measured with displaced sensors. EGS-AGU-EGU Joint Assembly, Nice, France, April 6–11, 2003, European Geophysical Union, Katlenburg-Lindau, Germany, (www.eol.ucar.edu/ horst/egs2003.html)
Horst TW, Weil JC (1994) How far is far enough? The fetch requirements for micrometeorological measurement of surface fluxes. J Atmos Ocean Technol 11:1018–1025

Horst TW, Kleissl J, Lenschow DH, Meneveau C, Moeng C, Parlange MB, Sullivan PP, Weil JC (2004) HATS: field observations to obtain spatially filtered turbulence fields from crosswind arrays of sonic anemometers in the atmospheric surface layer. J Atmos Sci 61:1566–1581

Kaimal JC, Gaynor JE (1991) Another look to sonic thermometry. Boundary-Layer Meteorol 56:401–410

Kanemasu ET, Verma SB, Smith EA, Fritschen LY, Wesely M, Fild RT, Kustas WP, Weaver H, Steawart YB, Geney R, Panin GN, Moncrieff JB (1992) Surface flux measurements in FIFE: an overview. J Geophys Res 97:18,547–18,555

Kohsiek W, Liebethal C, Vogt R, Oncley S, Bernhofer C, Foken T (2007) The energy balance experiment EBEX-2000. Part III: behaviour and quality of the radiation measurements. Boundary-Layer Meteorol 123, xx–xx

Koitzsch R, Dzingel M, Foken T, Mücket G (1988) Probleme der experimentellen Erfassung des Energieaustausches über Winterweizen. Z Meteorol 38:150–155

Kristensen L, Mann J, Oncley SP, Wyngaard JC (1997) How close is close enough when measuring scalar fluxes with displaced sensors? J Atmos Ocean Technol 14:814–821

Laubach J, Teichmann U (1996) Measuring energy budget components by eddy correlation: data corrections and application over low vegetation. Contr Atmos Phys 69:307–320

Lee X, Black TA (1993) Atmospheric turbulence within and above a Douglas-fir stand. Part II: eddy fluxes of sensible heat and water vapour. Boundary-Layer Meteorol 64:369–389

Lee X, Black TA (1994) Relating eddy correlation sensible heat flux to horizontal sensor separation in the unstable atmospheric surface layer. J Geophys Res 99(D9):18,545–18,553

Lee X, Massman WJ, Law B (eds.) (2004) Handbook of micrometeorology: a guide for surface flux measurement and analysis. Kluwer Academic Publishers, Dordrecht, 250 pp

Leuning R (2004) Measurements of trace gas fluxes in the atmosphere using eddy covariance: WPL correction revised. In: Lee X, Massman WJ, Law B (eds.), Handbook of micrometeorology: a guide for surface flux measurement and analysis. Kluwer Academic Publishers, Dordrecht, pp 119–132

Liebethal C, Foken T (2003) On the significance of the Webb correction to fluxes. Boundary-Layer Meteorol 109:99–106

Liebethal C, Foken T (2004) On the significance of the Webb correction to fluxes, Corrigendum. Boundary-Layer Meteorol 113:301

Liu H (2005) An alternative approach for $CO_2$ flux correction caused by heat and water vapour transfer. Boundary-Layer Meteorol 115:151–168

Liu H, Peters G, Foken T (2001) New equations for sonic temperature variance and buoyancy heat flux with an omnidirectional sonic anemometer. Boundary-Layer Meteorol 100:459–468

Massman WJ (2000) A simple method for estimating frequency response corrections for eddy covariance systems. Agric For Meteorol 104:185–198

Mauder M, Liebethal C, Göckede M, Leps J-P, Beyrich F, Foken T (2006) Processing and quality control of eddy covariance data during LITFASS-2003. Boundary-Layer Meteorol 121:67–88

Mauder M, Oncley SP, Vogt R, Weidinger T, Ribeiro L, Bernhofer C, Foken T, Kohsiek W, Liu H (2007) The Energy Balance Experiment EBEX-2000. Part II: intercomparison of turbulence sensors and processing methods. Boundary-Layer Meteorol 123, xx–xx

Milroy SP, Bange MP (2003) Nitrogen and light responses of cotton photosynthesis and implications for crop growth. Crop Sci 43:904–913

Moore CJ (1986) Frequency response corrections for eddy correlation systems. Boundary-Layer Meteorol 37:17–35

Oncley SP, Delany AC, Horst TW, Tans PP (1993) Verification of flux measurement using relaxed eddy accumulation. Atmos Environ 27:2417–2426

Panin GN, Tetzlaff G, Raabe A (1998) Inhomogeneity of the land surface and problems in the parametrization of surface fluxes in natural conditions. Theor Appl Climatol 60:163–178

Philip JR (1961) The theory of heat flux meters. J Geophys Res 66:571–579

Ruppert J, Thomas C, Foken T (2006) Scalar similarity for relaxed eddy accumulation methods. Boundary-Layer Meteorol 120:39–63

Schotanus P, Nieuwstadt FTM, DeBruin HAR (1983) Temperature measurement with a sonic anemometer and its application to heat and moisture fluctuations. Boundary-Layer Meteorol 26:81–93

Shuttleworth WJ (1993) Evaporation. In: Maidment DR (ed.), Handbook of hydrology. McGraw-Hill, New York, pp 4.1–4.53

Soong S-T, Tanrikulu S, Wilczak JM, Bao J-W, Martien PT, Michelson SA (2004) Simulation of an ozone episode during the Central California Ozone Study. Part II: CAMx air quality model simulations. 13th Joint conference on the applications of air pollution meteorology with the air and waste management association, Vancouver, BC, August 23–26, 2004. American Meteorological Society, 2.2

Tanner BD, Swiatek E, Greene JP (1993) Density fluctuations and use of the krypton hygrometer in surface flux measurements. In: Allen RG (ed.), Management of irrigation and drainage systems: integrated perspectives. American Society of Civil Engineers, New York, NY, pp 945–952

Tanrikulu S, Stauffer DR, Seaman NL, Ranzieri AJ (2000) A field-coherence technique for meteorological field-program design for air quality studies. Part II: evaluation in the San Joaquin Valley. J Appl Meteorol 39:317–334

Tsvang LR, Aligusejnov AK, Perepelkin VG, Sulev MA, Mee'lder ME, Zeleny Y (1987) Opyt zamykanije teplogo balansa v prizemnom sloe i na poverchnosti zemli. Izv Acad Sci USSR, Atmos Ocean Phys 23:3–13 [Attempt to close the energy balance in the near surface layer and at the soil surface]

Twine TE, Kustas WP, Norman JM, Cook DR, Houser PR, Meyers TP, Prueger JH, Starks PJ, Wesley ML (2000) Correcting eddy-covariance flux underestimates over a grassland. Agric For Meteorol 103:279–300

van Dijk A, Kohsiek W, DeBruin HAR (2003) Oxygen sensitivity of krypton and Lyman-alpha hygrometers. J Atmos Ocean Technol 20:143–151

Verma SB, Kim J, Clement RJ (1992) Momentum, water vapor, and carbon dioxide exchange at a centrally located prairie site during FIFE. J Geophys Res 97:18,629–18,639

Vickers D, Mahrt L (1997) Quality control and flux sampling problems for tower and aircraft data. J Atmos Ocean Technol 14:512–526

Webb EK, Pearman GI, Leuning R (1980) Correction of the flux measurements for density effects due to heat and water vapour transfer. Quart J Roy Meteorol Soc 106:85–100

Wilczak JM, Oncley SP, Stage SA (2001) Sonic anemometer tilt correction algorithms. Boundary-Layer Meteorol 99:127–150

Wilczak JM, Bao J-W, Michelson SA, Tanrikulu S, Soong S-T (2004) Simulation of an ozone episode during the Central California Ozone Study. Part I: MM5 meteorological model simulations. In: 13th Joint conference on the applications of air pollution meteorology with the air and waste management association, Vancouver, BC, August 23–26, 2004. American Meteorological Society, 2.1

Wilson K, Goldstein A, Falge E, Aubinet M, Baldocchi DD, Berbigier P, Bernhofer C, Ceulemans R, Dolman H, Field C, Grelle A, Ibrom A, Law BE, Kowalski A, Meyers TP, Moncrieff J, Monson R, Oechel W, Tenhunen J, Valentini R, Verma S (2002) Energy balance closure at FLUXNET sites. Agric For Meteorol 113:223–243

Wyngaard JC (1988) Flow-distortion effects on scalar flux measurements in the surface layer: implications for sensor design. Boundary-Layer Meteorol 42:19–26